Extending the Atmospheric River Concept to Aerosols:

Climate and Air Quality Impacts

Sudip Chakraborty[1*], Bin Guan[1,2], Duane E. Waliser[1], Arlindo Da Silva[3], Sophie Uluatam[4], Peter Hess[4]

[1]Jet Propulsion Laboratory, California Institute of Technology, Pasadena, CA
[2]Joint Institute for Regional Earth System Science and Engineering, University of California, Los Angeles, CA
[3] Global Modeling and Assimilation Office, NASA/Goddard Space Flight Center, Greenbelt, MD
[4] Cornell University, Ithaca, NY

*Corresponding Author

Abstract

Despite strong impacts that aerosols have on climate and air quality, significant gaps remain in our knowledge concerning their long-range transport, especially extreme transport events. With this consideration in mind and by leveraging the "atmospheric river" concept, this work develops an objective global algorithm for detecting aerosol atmospheric rivers (AARs), shows a climatology of AARs, elucidates their contributions to major global aerosol transport pathways, and illustrates how AARs can drive extreme cases of poor air quality conditions. Our methodology separately accounts for dust, carbonaceous (accounting for organic and black carbon separately where appropriate), sea salt and sulfate aerosols. Findings show there are a number of long-range regional transport pathways where AARs account for a sizable fraction (40-80%) of the total transport in relatively few events (20-40 AAR days/year). This study highlights the role of AARs in establishing source-receptor relationships that can drive regional air-quality and extremes.

Plain Language Summary

Aerosols play an important role in climate and air quality. They can influence climate through their interactions with clouds and precipitation, solar and infrared radiation, and also have adverse impacts on visibility and human health. However, such influences are not confined to their source regions as aerosols can be transported long distances, often across and between continents. This study develops an objective, global atmospheric aerosol rivers (AAR) detection algorithm to identify these narrow and elongated regions of extreme aerosol mass transport. We develop and show AAR climatologies for five major aerosol species, identify their major transport pathways across the globe, and provide a few recent examples of AARs that negatively impacted regional air quality. For the most impactful aerosol species (e.g. sea salt, dust, carbonaceous, sulfate), and for many regions of the globe, we show that a limited number of extreme cases (~20-40 days per year) of AARs contribute a large fraction (40-80%) of the total aerosol transport across a given region.

1. Introduction

Aerosols play an important role in climate by modulating radiative forcing via scattering and absorbing sunlight (direct effect)(Penner et al., 2001), precipitation (Chakraborty et al., 2018; Levy et al., 2013) by influencing cloud microphysics (Andreae & Rosenfeld, 2008) (indirect effect), and thus play an influential role in climate and climate change (M. O. Andreae & Rosenfeld, 2008; Fan et al., 2016; Stevens & Feingold, 2009), water availability and drought (Rosenfeld et al., 2008), and extreme weather events (Wang et al., 2020). Moreover, aerosols are known to degrade visibility and air quality, with the latter associated with small particulates that can impact the breathability of the air (Wang & Christopher, 2003) and negatively influence human health. In addition, agricultural dust can transport pathogens and impact crops, an example being *Fusarium Oxysporum*, the causal agent of Fusarium wilt that has been identified in both North African and Asian dust samples (Palmero et al., 2011; Yeo & Kim, 2002). Aerosols and their atmospheric precursors result from the emissions from biomass burning, industrial processes (Abel et al., 2003), biogenic processes (Andreae & Crutzen, 1997), and the impact of surface wind (Kim et al., 2014; Prospero et al., 2002) that extracts the aerosols over the oceans (sea salt) and land (dust). However, aerosol loadings and impacts are not confined to their emission regions since regional weather systems and global atmospheric circulation can transport aerosols far from their source regions.

Previously, many studies have identified and characterized long-range and intercontinental aerosol transport using various observational data sets (Prospero et al., 2010). Some examples include the transport of aerosols from biomass burning from East Asia to the tropical central Pacific (Eck et al., 2005), smoke from the Maritime Continent to the western

Pacific (Xian et al., 2013), and dust from the Sahara Desert to the Americas (Prospero et al., 2010) – a most recent example being the dust storm (referred to in the media as "Godzilla") that transported clouds of dust from the Sahara Desert to the Caribbean and the southeastern United States and significantly influenced the visibility index and air quality (https://www.cnn.com/2020/06/23/weather/saharan-dust-plume-caribbean-us-forecast/index.html).

Despite these findings, our current knowledge about long-range aerosol transport, particularly its extremes, largely relies on case studies and regional considerations and approaches (Prospero et al., 2002, 2010; Xian et al., 2013). A clear picture of the global, long-term climatology of aerosol transport events, especially the contributions from, and characteristic of, extreme events, has yet to be constructed. This gap derives from the challenges of developing the needed global observation datasets and the methodology to systematically and uniformly identify and analyze major aerosol transport events and pathways across the globe. Until now, a long-term global climatology of major aerosol transport events and pathways, including frequency of occurrence, mass transports of different aerosol species, and contributions of extreme transport events to the total aerosol transport, have not been available.

Over the last decade, there has been significant growth in studies (Lavers et al., 2011; Ralph et al., 2019; Neiman et al., 2008, 2011; F. M. Ralph et al., 2017; Ralph et al., n.d., 2005, 2006; Ralph et al., 2004) related to the narrow regions of enhanced horizontal water vapor transport, referred to as Atmospheric Rivers (ARs). These water vapor transport extremes not only shape the global energy and water cycles through their major contribution to the total poleward water vapor transport (Ralph et al., 2017; Zhu & Newell, 1998), but also shape the character of regional precipitation (Waliser & Guan, 2017), wind (Waliser & Guan, 2017) and

drought/flood across the globe (Guan & Waliser, 2015; Ralph & Dettinger, 2012; Waliser & Guan, 2017). The rapidly increasing number of AR-related studies in recent years illustrate recognition and acceptance of the AR phenomenological framework in the research and applications communities (Ralph et al., 2017). The success of the water vapor AR concept motivates the development and utilization of a similar approach for aerosols. This includes the means to objectively identify extreme aerosol transport events in a uniform manner across the globe, ideally using an observation-based dataset that accounts for but also distinguishes between different major aerosol species.

With the above motivations in mind, this study introduces the extension and application of an already established AR detection algorithm (Guan et al., 2018; Guan & Waliser, 2015, 2019) to aerosols as a new and an alternative approach for understanding and quantifying aerosol transport extremes, hereafter "Atmospheric Aerosol Rivers" (AARs). This AR detection algorithm was designed for global studies and detects ARs in the field of horizontal, column-integrated, water vapor transport based on a combination of intensity, geometric, and directional thresholds consistently applied globally. This global AR algorithm (Guan et al., 2018; Guan & Waliser, 2015) compares well with region-specific algorithms in terms of the basic characteristics of ARs (Eiras-Barca et al., 2018; Guan et al., 2018; Guan & Waliser, 2015; Yang et al., 2018), and has been widely used in the hydrometeorological and climate research communities (Chapman et al., 2019; Dhana Laskhmi & Satyanarayana, 2020; Edwards et al., 2020; Gibson et al., 2020; Guan et al., 2020a; Guan & Waliser, 2019; Huning et al., 2019; Jennrich et al., 2020; Nash & Carvalho, 2019; Sharma & Déry, 2020; Wang et al., 2020; Zhou & Kim, 2019). An example to illustrate the detection of an AR is shown in Figure 1 (discussed

later). The modifications to this AR algorithm that were developed and adopted in this study to detect AARs are described in the Methods section.

In this study, we apply the global AAR detection algorithm to version 2 of the Modern-Era Retrospective analysis for Research and Applications (MERRA-2) aerosol reanalysis (Gelaro et al., 2017) dataset. The MERRA-2 aerosol reanalysis performs reasonably well in capturing the global aerosol optical depth when compared with data from 793 Aerosol Robotic Network (AERONET) stations (Gueymard & Yang, 2020) and has already been used for aerosol transport-related studies (Sitnov et al., 2020; Xu et al., 2020). Our AAR detection algorithm is separately applied to dust (DU), carbonaceous (CA, with organic and black carbon, OC and BC, accounted for separately where appropriate), sulfate (SO_4 or SU), and sea salt (SS) aerosol species (Gelaro et al., 2017). Based on application of this AAR detection algorithm to MERRA-2 for these five aerosol species, we construct and describe global climatological features of AARs, including their mean frequency and transport values, AAR contributions to major pathways of intra- and inter-continental aerosol transport, and illustrate and discuss a few AAR events that resulted in significant impacts on regional air quality.

2. Data and Modification of the AR algorithm to detect AARs:

We use hourly averaged surface and vertically integrated variables from MERRA-2 aerosol reanalysis data (tavg1_2d_aer_Nx – 2D) available for the public to download at https://disc.gsfc.nasa.gov/datasets/M2T1NXAER_5.12.4/summary. The horizontal resolution of the data is 0.5° x 0.625°. We use the zonal (U) and meridional (V) components of the IAT (kg m^{-1} s^{-1}) for five different species, DU, SS, BC, OC, and SU. For example, the parameter BCFLUXU in the data set denotes the black carbon IAT. Total IAT is calculated from the U and V components as

$$IAT_n = \sqrt[2]{IATU_n^2 + IATV_n^2}$$

where n indicates each of the five aerosol species, and U and V denote zonal and meridional components of IAT.

There are five steps in the algorithm to identify AARs, largely similar to the AR detection steps described in detail in Guan and Waliser (Guan & Waliser, 2015). The requirements implemented in each step of AAR detection are as follows: 1) IAT at each grid cell is greater than the seasonally- and regionally-dependent 85th percentile, based on which contiguous areas ("objects") of enhanced IAT are isolated; 2) within each object, IAT directions at individual grid cells are consistent with the object-mean IAT over at least 50% of the surface area of the object, i.e., the IAT directions are largely coherent within a given object; 3) object-mean IAT is greater than the median of all candidate objects from the previous step, i.e., retaining only the stronger 50% of the objects from step 3; 4) the direction of object-mean IAT is consistent with (within 45° of) the orientation of the shape of the object, i.e., requiring the object-mean IAT to be directed along river (as opposed to across river); and 5) object length is greater than 2000 km and length-to-width ratio greater than 2. Objects retained after these five steps are the defined set of AARs used in this study. Compared to our AR algorithm, the AAR algorithm described above has two slight modifications. In the AR algorithm, in addition to the 85th percentile of integrated water vapor transport (IVT), a fixed lower limit of IVT (i.e., 100 kg m^{-1} s^{-1}), is applied in step 1 to facilitate the detection of ARs in the polar regions where IVT is extremely weak climatologically. It is found a fixed lower limit was not necessary in the AAR algorithm and therefore only the 85th percentile limit is applied in step 1. In step 3 of the AAR algorithm, instead of thresholding only the meridional mass flux as in the AR algorithm, we threshold the total mass flux since it is expected that AARs can transport aerosols in any direction, unlike ARs

that are known to transport water vapor primarily in the poleward direction given the overall moisture gradient between the tropics and extratropics. To detect the DU AAR during the dust storm Godzilla (Fig. 4A), we have used hourly averaged IAT data available at a resolution of 0.25° from https://opendap.nccs.nasa.gov/dods/GEOS-5/fp/0.25_deg/assim. The true-color image on AOT (Fig. 1C) is obtained from a nature run from the GEOS-FP system from https://g5nr.nccs.nasa.gov/images/aerosols/. Since the NR data have a higher resolution, they are more useful for concept illustration purposes. We have used AERONET (https://aeronet.gsfc.nasa.gov) datasets to estimate the changes in AOT (Fig. 4). We have used the river discharge data from https://waterdata.usgs.gov to estimate the Feather River's discharge in Oroville, CA. SSMIS data (http://ghrc.nsstc.nasa.gov/hydro/) were used to plot Figure 1A.

3. Detection of AARs: Leveraging the AR construct and methodologies:

We begin by showing examples of satellite-based observations of AR signatures in water vapor content, their formal detection by the AR algorithm using water vapor transport, and analogous examples for AARs. Figure 1A shows a global, satellite-observed map of integrated water vapor (IWV) on 02/06/2007 from the Special Sensor Microwave Imager/Sounder (SSMIS). This date was selected to highlight the AR in northern California that, along with other ARs in the same area around that time period, led to the delivery of a torrential amount of precipitation leading to major spillway damage of the Oroville Dam and associated downstream flooding (Henn et al., 2020). The enclosed area in Fig. 1A shows a region of high IWV near the Californian coast suggestive of AR conditions. The AR algorithm (Guan & Waliser, 2015) detects several ARs on that day across the globe, including an AR extending from 180°W to 100°W with IVT> 600 $kgm^{-1}s^{-1}$ and making landfall over the northern California region (Fig. 1B). This landfalling AR near the Californian coast produced a torrent of rain that increased the

Feather River discharge from < 10,000 cu ft/sec to 110,000 cu ft/sec (Fig. S1) and caused the failure of the main and emergency spillways leading to massive flooding and local evacuations.

To illustrate the viability of our AAR algorithm, with analogy to the AR example, Fig. 1C depicts aerosol optical thickness (AOT) data from the Goddard Earth Observing System, Version 5 Nature Run (Gelaro R, Putman WM, Pawson S, 2015) (a more recent version of the model used for the MERRA-2 aerosol reanalysis) for 08/18/2006. This example highlights four narrow regions of high aerosol AOT: a region of high DU AOT extending from the Sahara Desert to the Atlantic Ocean to the west and Europe to the north (area enclosed by an orange ellipse), a narrow stretch of high CA AOT originating from the Amazon rainforest and flowing east towards the South Atlantic Ocean (green ellipse), a region of high SS concentration right over the Southern Ocean (blue ellipse), and a region of high SU AOT detected over the northwestern Pacific Ocean between the east coast of China and Siberia (black ellipse). Figure 1D shows AARs identified by the AAR algorithm based on integrated aerosol transport (IAT) on the same day over four locations that correspond to the high AOT locations discussed above. This includes a DU AAR indicating a region of high dust aerosol transport detected over the high dust AOT region shown in Figure 1C. Similarly, an SU AAR extending from north of Japan to the southern Siberian region is detected, an SS AAR is identified over the region of high SS AOT over the Southern Ocean, and a CA AAR is detected over the South Atlantic Ocean. Such AARs denote the existence of narrow stretches of enhanced aerosol transport within the high AOT regions of different aerosol species.

4. AAR climatology:

Based on the collection of individual AARs detected by our algorithm (as illustrated above) over the years 1997-2014, we now examine their climatology, including the frequency of

occurrence and the amount of mass transported by those AARs. For reference, Figure 2A shows the global climatology of AR frequency (shaded) and IVT (arrows). The average number of AR days per year are notably higher over the mid-latitude oceans, signifying their role in the water vapor transport from the tropics to the extratropics (Guan et al., 2020b; Guan & Waliser, 2015; F. M. Ralph & Dettinger, 2012; F. Martin Ralph et al., 2017) and from the ocean to land. The largest AR frequency is noted over the North Pacific/Atlantic, southeastern Pacific, South Atlantic, and the Southern Oceans where AR frequency exceeds 40 days per year with mean AR IVT exceeding 250 $kgm^{-1}s^{-1}$.

In Figs. 2B-2F, we show AAR climatologies for different species of aerosols. The Sahara Desert, with a strong anticyclonic and diverging circulation pattern, helps to generate many AARs that transport DU in a number of directions (Fig. 2B). A significant number (~30 days/year) of DU AARs emerge from the Saharan Desert, flow across the tropical North Atlantic to the Caribbean, and transport large amounts of dust (mean IAT by DU AARs ~3 x 10^{-3} $kgm^{-1}s^{-1}$). Other regions with frequent occurrence of DU AARs include China, the deserts of Mongolia, and Kazakhstan, and the subtropical desertic regions of the Middle East, accumulating ~40 DU AAR days per year that travel over the northern North Pacific and reach western North America, but with a lower mean mass flux compared to the Sahara-Caribbean pathway.

To put the IAT associated with AARs in context, we compare it to the annual total IAT. Zonally averaged total IAT for dust (i.e., all directions of transport considered) in the Northern (Southern) Hemisphere peaks around 45°N (45°S) with a maximum IAT of ~250 x 10^{-6} $kgm^{-1}s^{-1}$ (150 x 10^{-6} kg $m^{-1}s^{-1}$), presumably in large part due to the latitudes of the deserts (Fig. 3A). Total IAT rapidly increases between 25°N and 45°N (Fig. 3A), and DU AARs contribute to the largest fraction (around 80%, Fig. 3A) of total IAT in this latitude band, indicating the strong influence

of the Sahara desert dust source on the pattern of global dust transports (Prospero et al., 2002). In the Southern Hemisphere, DU AARs are fewer but not uncommon, where the Patagonia region and Namibia generate a large number of DU AARs (~25 days/year).

The major sources of CA (Figs. 2C and 2E) AARs are forest fires and anthropogenic emission; the latter include fossil fuel burning and agricultural burning. As a result, higher population regions like Europe, eastern US, industrialized areas over eastern China and North India, as well as the rainforests over the Congo and southern Amazon, are associated with numerous BC AARs (20-40 days/year; Fig. 2C) that transport BC aerosols either in the direction of the trade winds in the tropics and subtropics or the westerlies in the midlatitudes. OC AARs (Fig. 2E) show a similar pattern as in BC AARs, but with a lower frequency than in the case of BC.

Unlike DU and CA AARs with primary sources over the land, the SS AARs (Fig. 2D), expectedly, are closely associated with oceanic regions. Many SS AARs exist over the tropical oceans, and especially over the subtropical trade wind regions. Owing to the facts that SS particles are larger, typically confined to the planetary boundary layer (Gross & Baklanov, 2007), and may not travel long distances, such AARs suggest emissions of SS aerosols result from high wind speed and surface evaporation along the storm tracks (May et al., 2016; Sofiev et al., 2011). Over the midlatitudes and in the Southern Ocean, SS AARs follow the storm tracks and are somewhat similar to AR pathways, although the imprint of the climatological features of the surface wind field (e.g. separation between easterly trades and mid-latitude westerlies) are more strongly evident in the SS AAR climatology (comparing Fig. 2D to Fig. 2A). Along the midlatitude storm tracks, SS (~20 days/year) AAR transports are directed from the eastern Pacific Ocean region to the west coast of the United States and from northern Atlantic Ocean to

Europe. Mean IAT values for SS AARs are higher (~1 x 10^{-3} $kgm^{-1}s^{-1}$) over the midlatitude oceans than over the subtropical oceans (~0.5 x 10^{-3} $kgm^{-1}s^{-1}$), whereas the frequency of SS AARs is higher over the subtropical oceans. Over the Indian Ocean, SS AARs and the directions of SS transport follow the India-Oceania summer monsoon pathway.

SU AARs occur more frequently (~40 days/year, Fig. 2F) in the Northern Hemisphere and over the South Indian, South Atlantic, and Southern Oceans with an average IAT ~0.4 x 10^{-3} $kgm^{-1}s^{-1}$. Many SU AARs are also located over the eastern US, Europe, and eastern China in the midlatitude region owing to anthropogenic emissions as well as biogenic activities in these regions.

Analogous to the substantial role that ARs have on the total transport of water vapor (accounting for over 90% of the total poleward transport in the midlatitudes), AAR transports, when zonally-averaged, contribute up to ~40% of the total IAT (i.e., all directions of transport considered) for SU and CA over most latitudes, about 80% for DU between 25°N and 45°N (as discussed earlier), and about 60% for SS over the Southern Ocean (Fig. 3). Thus, AARs account for a substantial fraction of the transport of aerosol mass across the globe.

5. Case studies of recent AAR events with societal impacts

Figure 4 shows specific cases of DU (Fig. 4A) and CA (Fig. 4C) AARs, with an indication of their impact on air quality. Figure 4A shows one DU AAR detected on June 25, 2020 associated with the recent dust storm event that extended from the Sahara Desert to the southern/southeastern United States through the Caribbean. The dust event, named "Godzilla" in media reports (https://www.usatoday.com/story/news/nation/2020/06/24/sahara-dust-storm-us-gulf-coast-texas-what-to-expect/3250102001/) owing to its gigantic size, darkened the skies over the Caribbean and the United States. From our analysis, a large and strong DU AAR is detected

with IAT of ~ 30 x 10^{-3} $kgm^{-1}s^{-1}$, which is about four orders of magnitude higher than the climatological IAT of DU AARs (200 x 10^{-6} $kgm^{-1}s^{-1}$) in that latitude range (Fig. 3A). As this event reached Tallahassee, Florida, an AERONET station recorded a spike in the total AOT at 500 nm from 0.2 before the arrival of the AAR to 1.6 on and after 23rd June for several days. The largest contributor to the aerosol concentrations was from the coarse, rather than the fine, aerosol mode, indicating a large increase in dust particles (Fig. 4B). Another AERONET station located in Cape San Juan in Puerto Rico, along the dust storm's route to the United States, recorded a similar increase in the coarse mode and total AOT from <0.2 to above 1.5 after 20th June (not shown).

Deforestation has threatened the conservation of the rainforest (de Area Leão Pereira et al., 2019) and has catalyzed a number of massive fire events in August 2019 (Silva Junior et al., 2020) (28% more than in 2018). Such fire events have acted as a source to many CA and SU AARs during August 2019. We show one of those CA (Fig. 4C) and SU AARs (Fig. S2) as identified by our AAR algorithm. On August 18, 2019, a massive, ~13,000 km long CA AAR coexisting with an SU AAR, with greater than 1 x 10^{-3} $kgm^{-1}s^{-1}$ of CA and ~0.25 x 10^{-3} $kgm^{-1}s^{-1}$ of SU aerosols extended between the eastern tropical Pacific Ocean and the South Atlantic Ocean. São Paulo, a city far from the Amazon's fire region, recorded an increase in the aerosol fine mode amount as well as the total AOT at 500 mm rising from 0.2 to 1 after 17th August, in association with the AAR (Fig. 4D). Another AERONET station located in central Brazil (not shown) measured a similar and steady rise in the fine aerosol concentration from pristine (AOT <0.1) to polluted conditions (AOT ~1.0).

6. Concluding remarks

By extending the concept of water vapor ARs to aerosols, this study offers an additional framework for studying extreme transports of aerosols via atmospheric aerosol rivers (AARs), giving initial indications of their influences on aerosol-related climate features and air quality. Using an algorithm originally developed to detect ARs with a few modifications (see Method), AARs of five different species are detected using aerosol mass flux data from the MERRA-2 reanalysis. From these results, we constructed and examined the climatology of AAR frequency and transport and identified the regions where relatively few AAR events account for notable fractions of the total aerosol transport.

Our results show that AARs are responsible for transporting greater than 40% of the total IAT over many tropical and mid-latitude regions. Among these, DU AARs that originate from the deserts over the Northern Hemisphere transport greater than 80% of total dust IAT between 25°N-45°N, and SS AARs over the Southern Ocean transport about 60% of the total IAT. These results show that 20-40 AAR days per year contribute to a large fraction of the total aerosol transport in many regions of the globe. To our knowledge, our study represents the first to apply and extend the concept of "atmospheric rivers" to understanding the role and characteristics of extreme and long-range aerosol transport events in global aerosol climate and air quality.

Apart from AARs contribution to global aerosol transport, an additional feature of interest is the potential societal impacts of AARs, including their role in considerations of source-receptor (Clappier et al., 2015) relationships and associated impacts on air quality. Examples examined included a DU AAR that originated from the Sahara Desert and impacted AOT concentration over Tallahassee, Florida (the June 24, 2020 "Godzilla" dust storm), and a CA AAR that originated from a forest fire in the Amazon rainforest and raised fine mode aerosol

particle concentrations over São Paulo. Besides their impact on air quality, aerosols can also attenuate sunlight by scattering, absorbing, and reflecting the incoming shortwave energy. For example, the same DU AAR mentioned above that originated from the Sahara Desert caused the darkening of skies over the Caribbean and southeastern United States.

These specific cases, along with the climatological results, emphasize a critical role of AARs on source-receptor relationships (Clappier et al., 2015), and suggest substantive impacts by AARs on local air quality, climate and radiative forcing conditions over regions far from their source regions. Our study is intended to introduce and highlight the potential value of the AR concept to the study of aerosol transport extremes and their impacts on the global climate and air quality. Future studies on AARs may involve the identification of their role on radiative forcing patterns, as well as cloud and precipitation development, and further examination of the characteristics and processes associated with AAR events that result in notable impacts on local air quality.

Acknowledgements:

This work was supported by the National Aeronautics and Space Administration. The contribution of S.C. and D.W. was carried out on behalf of the Jet Propulsion Laboratory, California Institute of Technology, under a contract with NASA. All the data are publicly available and free to download. Please see section 2 for the links to all the data sets used in this study. No new data have been created or used. The AAR code is available from B.G. on request.

References

Abel, S. J., Haywood, J. M., Highwood, E. J., Li, J., & Buseck, P. R. (2003). Evolution of biomass burning aerosol properties from an agricultural fire in southern Africa. *Geophysical Research Letters*. https://doi.org/10.1029/2003GL017342

Andreae, M. O., & Rosenfeld, D. (2008). Aerosol-cloud-precipitation interactions. Part 1. The nature and sources of cloud-active aerosols. *Earth-Science Reviews*. https://doi.org/10.1016/j.earscirev.2008.03.001

Andreae, Meinrat O., & Crutzen, P. J. (1997). Atmospheric aerosols: Biogeochemical sources and role in atmospheric chemistry. *Science*. https://doi.org/10.1126/science.276.5315.1052

de Area Leão Pereira, E. J., Silveira Ferreira, P. J., de Santana Ribeiro, L. C., Sabadini Carvalho, T., & de Barros Pereira, H. B. (2019). Policy in Brazil (2016–2019) threaten conservation of the Amazon rainforest. *Environmental Science & Policy*, *100*, 8–12. https://doi.org/https://doi.org/10.1016/j.envsci.2019.06.001

Chakraborty, S., Fu, R., Rosenfeld, D., & Massie, S. T. (2018). The Influence of Aerosols and Meteorological Conditions on the Total Rain Volume of the Mesoscale Convective Systems Over Tropical Continents. *Geophysical Research Letters*, *45*(23), 13,13-99,106. https://doi.org/10.1029/2018GL080371

Chapman, W. E., Subramanian, A. C., Delle Monache, L., Xie, S. P., & Ralph, F. M. (2019). Improving Atmospheric River Forecasts With Machine Learning. *Geophysical Research Letters*. https://doi.org/10.1029/2019GL083662

Clappier, A., Pisoni, E., & Thunis, P. (2015). A new approach to design source-receptor relationships for air quality modelling. *Environmental Modelling and Software*. https://doi.org/10.1016/j.envsoft.2015.09.007

Dhana Laskhmi, D., & Satyanarayana, A. N. V. (2020). Climatology of landfalling atmospheric Rivers and associated heavy precipitation over the Indian coastal regions. *International Journal of Climatology*. https://doi.org/10.1002/joc.6540

Eck, T. F., Holben, B. N., Dubovik, O., Smirnov, A., Goloub, P., Chen, H. B., et al. (2005). Columnar aerosol optical properties at AERONET sites in central eastern Asia and aerosol transport to the tropical mid-Pacific. *Journal of Geophysical Research: Atmospheres*, *110*(D6). https://doi.org/10.1029/2004JD005274

Edwards, T. K., Smith, L. M., & Stechmann, S. N. (2020). Atmospheric rivers and water fluxes in precipitating quasi-geostrophic turbulence. *Quarterly Journal of the Royal Meteorological Society*. https://doi.org/10.1002/qj.3777

Eiras-Barca, J., Ramos, A. M., Pinto, J. G., Trigo, R. M., Liberato, M. L. R., & Miguez-Macho, G. (2018). The concurrence of atmospheric rivers and explosive cyclogenesis in the North Atlantic and North Pacific basins. *Earth System Dynamics*. https://doi.org/10.5194/esd-9-91-2018

Fan, J., Wang, Y., Rosenfeld, D., & Liu, X. (2016). Review of aerosol-cloud interactions: Mechanisms, significance, and challenges. *Journal of the Atmospheric Sciences*. https://doi.org/10.1175/JAS-D-16-0037.1

Gelaro R, Putman WM, Pawson S, et al. (2015). Evaluation of the 7-km GEOS-5 nature run. *NASA Tech Rep Ser Glob Model Data Assim*, *36:1-305*.

Gelaro, R., McCarty, W., Suárez, M. J., Todling, R., Molod, A., Takacs, L., et al. (2017). The

Modern-Era Retrospective Analysis for Research and Applications, Version 2 (MERRA-2). *Journal of Climate*, *30*(14), 5419–5454. https://doi.org/10.1175/JCLI-D-16-0758.1

Gibson, P. B., Waliser, D. E., Guan, B., Deflorio, M. J., Ralph, F. M., & Swain, D. L. (2020). Ridging associated with Drought across the Western and Southwestern United States: Characteristics, trends, and predictability sources. *Journal of Climate*. https://doi.org/10.1175/JCLI-D-19-0439.1

Gross, A., & Baklanov, A. (2007). Aerosol Production in the Marine Boundary Layer Due to Emissions from DMS: Study Based on Theoretical Scenarios Guided by Field Campaign Data. In *Air Pollution Modeling and Its Application XVII*. https://doi.org/10.1007/978-0-387-68854-1_31

Guan, B., & Waliser, D. E. (2015). Detection of atmospheric rivers: Evaluation and application of an algorithm for global studies. *Journal of Geophysical Research*. https://doi.org/10.1002/2015JD024257

Guan, B., & Waliser, D. E. (2019). Tracking Atmospheric Rivers Globally: Spatial Distributions and Temporal Evolution of Life Cycle Characteristics. *Journal of Geophysical Research: Atmospheres*. https://doi.org/10.1029/2019JD031205

Guan, B., Waliser, D. E., & Martin Ralph, F. (2018). An intercomparison between reanalysis and dropsonde observations of the total water vapor transport in individual atmospheric rivers. *Journal of Hydrometeorology*. https://doi.org/10.1175/JHM-D-17-0114.1

Guan, B., Waliser, D. E., & Ralph, F. M. (2020a). A multimodel evaluation of the water vapor budget in atmospheric rivers. *Annals of the New York Academy of Sciences*. https://doi.org/10.1111/nyas.14368

Guan, B., Waliser, D. E., & Ralph, F. M. (2020b). A multimodel evaluation of the water vapor budget in atmospheric rivers. *Annals of the New York Academy of Sciences*. https://doi.org/10.1111/nyas.14368

Gueymard, C. A., & Yang, D. (2020). Worldwide validation of CAMS and MERRA-2 reanalysis aerosol optical depth products using 15 years of AERONET observations. *Atmospheric Environment*. https://doi.org/10.1016/j.atmosenv.2019.117216

Henn, B., Musselman, K. N., Lestak, L., Ralph, F. M., & Molotch, N. P. (2020). Extreme Runoff Generation From Atmospheric River Driven Snowmelt During the 2017 Oroville Dam Spillways Incident. *Geophysical Research Letters*, *47*(14), e2020GL088189. https://doi.org/10.1029/2020GL088189

Huning, L. S., Guan, B., Waliser, D. E., & Lettenmaier, D. P. (2019). Sensitivity of Seasonal Snowfall Attribution to Atmospheric Rivers and Their Reanalysis-Based Detection. *Geophysical Research Letters*. https://doi.org/10.1029/2018GL080783

Jennrich, G. C., Furtado, J. C., Basara, J. B., & Martin, E. R. (2020). Synoptic Characteristics of 14-Day Extreme Precipitation Events across the United States. *Journal of Climate*. https://doi.org/10.1175/JCLI-D-19-0563.1

Kim, D., Chin, M., Yu, H., Diehl, T., Tan, Q., Kahn, R. A., et al. (2014). Sources, sinks, and transatlantic transport of North African dust aerosol: A multimodel analysis and comparison with remote sensing data. *Journal of Geophysical Research: Atmospheres*, *119*(10), 6259–6277. https://doi.org/10.1002/2013JD021099

Lavers, D. A., Allan, R. P., Wood, E. F., Villarini, G., Brayshaw, D. J., & Wade, A. J. (2011). Winter floods in Britain are connected to atmospheric rivers. *Geophysical Research Letters*. https://doi.org/10.1029/2011GL049783

Levy, H., Horowitz, L. W., Schwarzkopf, M. D., Ming, Y., Golaz, J. C., Naik, V., &

Ramaswamy, V. (2013). The roles of aerosol direct and indirect effects in past and future climate change. *Journal of Geophysical Research Atmospheres*. https://doi.org/10.1002/jgrd.50192

Martin Ralph, F., Rutz, J. J., Cordeira, J. M., Dettinger, M., Anderson, M., Reynolds, D., et al. (2019). A scale to characterize the strength and impacts of atmospheric rivers. *Bulletin of the American Meteorological Society*. https://doi.org/10.1175/BAMS-D-18-0023.1

May, N. W., Quinn, P. K., McNamara, S. M., & Pratt, K. A. (2016). Multiyear study of the dependence of sea salt aerosol on wind speed and sea ice conditions in the coastal Arctic. *Journal of Geophysical Research*. https://doi.org/10.1002/2016JD025273

Nash, D., & Carvalho, L. (2019). Brief Communication: An Electrifying Atmospheric River: Understanding the Thunderstorm Event in Santa Barbara County during March 2019. *Natural Hazards and Earth System Sciences*. https://doi.org/10.5194/nhess-2019-342

Neiman, P. J., Ralph, F. M., Wick, G. A., Lundquist, J. D., & Dettinger, M. D. (2008). Meteorological Characteristics and Overland Precipitation Impacts of Atmospheric Rivers Affecting the West Coast of North America Based on Eight Years of SSM/I Satellite Observations. *Journal of Hydrometeorology*, *9*(1), 22–47. https://doi.org/10.1175/2007JHM855.1

Neiman, P. J., Schick, L. J., Martin Ralph, F., Hughes, M., & Wick, G. A. (2011). Flooding in western washington: The connection to atmospheric rivers. *Journal of Hydrometeorology*. https://doi.org/10.1175/2011JHM1358.1

Palmero, D., Rodríguez, J. M., De Cara, M., Camacho, F., Iglesias, C., & Tello, J. C. (2011). Fungal microbiota from rain water and pathogenicity of Fusarium species isolated from atmospheric dust and rainfall dust. In *Journal of Industrial Microbiology and Biotechnology*. https://doi.org/10.1007/s10295-010-0831-5

Penner, J. E., Andreae, M., Annegarn, H., Barrie, L., Feichter, J., Hegg, D., et al. (2001). Aerosols, their Direct and Indirect Effects. In *Climate Change 2001: The Scientific Basis. Contribution of Working Group I to the Third Assessment Report of the Intergovernmental Panel on Climate Change*. https://doi.org/10.1029/JD091iD01p01089

Prospero, J. M., Ginoux, P., Torres, O., Nicholson, S. E., & Gill, T. E. (2002). Environmental characterization of global sources of atmospheric soil dust identified with the Nimbus 7 Total Ozone Mapping Spectrometer (TOMS) absorbing aerosol product. *Reviews of Geophysics*. https://doi.org/10.1029/2000RG000095

Prospero, J. M., Landing, W. M., & Schulz, M. (2010). African dust deposition to Florida: Temporal and spatial variability and comparisons to models. *Journal of Geophysical Research: Atmospheres*, *115*(D13). https://doi.org/10.1029/2009JD012773

Ralph, F. M., & Dettinger, M. D. (2012). Historical and national perspectives on extreme west coast precipitation associated with atmospheric rivers during december 2010. *Bulletin of the American Meteorological Society*. https://doi.org/10.1175/BAMS-D-11-00188.1

Ralph, F. M., Dettinger, M., Lavers, D., Gorodetskaya, I. V., Martin, A., Viale, M., et al. (2017). Atmospheric rivers emerge as a global science and applications focus. In *Bulletin of the American Meteorological Society*. https://doi.org/10.1175/BAMS-D-16-0262.1

Ralph, F. Martin, Dettinger, M. D., Rutz, J. J., & Waliser, D. E. (n.d.). *Atmospheric Rivers* (2020th ed.). https://doi.org/10.1007/978-3-030-28906-5

Ralph, F. Martin, Neiman, P. J., & Rotunno, R. (2005). Dropsonde observations in low-level jets over the northeastern Pacific Ocean from CALJET-1998 and PACJET-2001: Mean vertical-profile and atmospheric-river characteristics. *Monthly Weather Review*.

https://doi.org/10.1175/MWR2896.1
Ralph, F. Martin, Neiman, P. J., Wick, G. A., Gutman, S. I., Dettinger, M. D., Cayan, D. R., & White, A. B. (2006). Flooding on California's Russian River: Role of atmospheric rivers. *Geophysical Research Letters*. https://doi.org/10.1029/2006GL026689
Ralph, F. Martin, Iacobellis, S. F., Neiman, P. J., Cordeira, J. M., Spackman, J. R., Waliser, D. E., et al. (2017). Dropsonde observations of total integrated water vapor transport within North Pacific atmospheric rivers. *Journal of Hydrometeorology*. https://doi.org/10.1175/JHM-D-17-0036.1
Ralph, F Martin, Neiman, P. J., & Wick, G. A. (2004). Satellite and CALJET Aircraft Observations of Atmospheric Rivers over the Eastern North Pacific Ocean during the Winter of 1997/98. *Monthly Weather Review*, *132*(7), 1721–1745. https://doi.org/10.1175/1520-0493(2004)132<1721:SACAOO>2.0.CO;2
Rosenfeld, D., Lohmann, U., Raga, G. B., O'Dowd, C. D., Kulmala, M., Fuzzi, S., et al. (2008). Flood or Drought: How Do Aerosols Affect Precipitation? *Science*, *321*(5894), 1309 LP – 1313. https://doi.org/10.1126/science.1160606
Sharma, A. R., & Déry, S. J. (2020). Variability and trends of landfalling atmospheric rivers along the Pacific Coast of northwestern North America. *International Journal of Climatology*. https://doi.org/10.1002/joc.6227
Silva Junior, C. H. L., Celentano, D., Rousseau, G. X., de Moura, E. G., Varga, I. van D., Martinez, C., & Martins, M. B. (2020). Amazon forest on the edge of collapse in the Maranhão State, Brazil. *Land Use Policy*, *97*, 104806. https://doi.org/https://doi.org/10.1016/j.landusepol.2020.104806
Sitnov, S. A., Mokhov, I. I., & Likhosherstova, A. A. (2020). Exploring large-scale black-carbon air pollution over Northern Eurasia in summer 2016 using MERRA-2 reanalysis data. *Atmospheric Research*. https://doi.org/10.1016/j.atmosres.2019.104763
Sofiev, M., Soares, J., Prank, M., De Leeuw, G., & Kukkonen, J. (2011). A regional-to-global model of emission and transport of sea salt particles in the atmosphere. *Journal of Geophysical Research Atmospheres*. https://doi.org/10.1029/2010JD014713
Stevens, B., & Feingold, G. (2009). Untangling aerosol effects on clouds and precipitation in a buffered system. *Nature*. https://doi.org/10.1038/nature08281
Waliser, D., & Guan, B. (2017). Extreme winds and precipitation during landfall of atmospheric rivers. *Nature Geoscience*. https://doi.org/10.1038/ngeo2894
Wang, J., & Christopher, S. A. (2003). Intercomparison between satellite-derived aerosol optical thickness and PM2.5 mass: Implications for air quality studies. *Geophysical Research Letters*. https://doi.org/10.1029/2003GL018174
Wang, Y., Le, T., Chen, G., Yung, Y. L., Su, H., Seinfeld, J. H., & Jiang, J. H. (2020). Publisher Correction: Reduced European aerosol emissions suppress winter extremes over northern Eurasia (Nature Climate Change, (2020), 10, 3, (225-230), 10.1038/s41558-020-0693-4). *Nature Climate Change*. https://doi.org/10.1038/s41558-020-0800-6
Wang, Z., Walsh, J., Szymborski, S., & Peng, M. (2020). Rapid arctic sea ice loss on the synoptic time scale and related atmospheric circulation anomalies. *Journal of Climate*. https://doi.org/10.1175/JCLI-D-19-0528.1
Xian, P., Reid, J. S., Atwood, S. A., Johnson, R. S., Hyer, E. J., Westphal, D. L., & Sessions, W. (2013). Smoke aerosol transport patterns over the Maritime Continent. *Atmospheric Research*, *122*, 469–485. https://doi.org/https://doi.org/10.1016/j.atmosres.2012.05.006
Xu, X., Wu, H., Yang, X., & Xie, L. (2020). Distribution and transport characteristics of dust

aerosol over Tibetan Plateau and Taklimakan Desert in China using MERRA-2 and CALIPSO data. *Atmospheric Environment*. https://doi.org/10.1016/j.atmosenv.2020.117670
Yang, Y., Zhao, T., Ni, G., & Sun, T. (2018). Atmospheric rivers over the Bay of Bengal lead to northern Indian extreme rainfall. *International Journal of Climatology*. https://doi.org/10.1002/joc.5229
Yeo, H. G., & Kim, J. H. (2002). SPM and fungal spores in the ambient air of west Korea during the Asian dust (Yellow sand) period. *Atmospheric Environment*. https://doi.org/10.1016/S1352-2310(02)00672-6
Zhou, Y., & Kim, H. (2019). Impact of Distinct Origin Locations on the Life Cycles of Landfalling Atmospheric Rivers Over the U.S. West Coast. *Journal of Geophysical Research: Atmospheres*. https://doi.org/10.1029/2019JD031218
Zhu, Y., & Newell, R. E. (1998). A proposed algorithm for moisture fluxes from atmospheric rivers. *Monthly Weather Review*. https://doi.org/10.1175/1520-0493(1998)126<0725:APAFMF>2.0.CO;2

Figure Captions

Figure 1. (A) SSMI/S satellite observation of integrated water vapor (IWV; mm) for 02/06/2017 showing signatures of ARs. (B) ARs detected based on integrated water vapor (IVT; $kgm^{-1}s^{-1}$) on the same day. The AR corresponding to the region of enhanced IWV marked by the ellipse in (A) was responsible for notable landfall impact over the US West Coast. (C) GEOS-FP aerosol extinction AOT for different aerosol species on 08/18/2006 showing signatures of AARs. (D) AARs of different aerosol species detected by the AAR algorithm based on integrated aerosol transport (IAT; $kgm^{-1}s^{-1}$). The IAT-based AARs correspond to regions with high aerosol concentrations marked by the ellipses in (C). Grey: sulfate; Green: Carbonaceous or organic and black carbon; Blue: sea salt; Orange: dust. Color bars show the magnitude of IVT ($kg\ m^{-1}s^{-1}$) and IAT ($10^{-3}\ kg\ m^{-1}s^{-1}$).

Figure 2. Climatological frequency (days/year; shading) and transport (arrows; $kg\ m^{-1}\ s^{-1}$) of (A) ARs and (B-F) AARs during 1997-2014 based on MERRA-2. (B) Dust; (C) Black carbon; (D) Sea salt; (E) Organic carbon; (F) Sulfate.

Figure 3. Zonally averaged total IAT ($10^{-6}\ kgm^{-1}s^{-1}$; dashed line) and the part of the total IAT associated with the AARs (solid line) for five different species of aerosols between 1997-2014. Dotted lines show the fractional contribution of AARs to the total IAT.

Figure 4. (A) Dust AAR detected by the AAR algorithm from GEOS-FP showing the amount of dusts transported ($10^{-3}\ kg\ m^{-1}\ s^{-1}$) from the Saharan Desert to Florida on 06/25/2020 at 1330 UTC. (B) Coarse mode AOT, fine mode AOT, and total AOT at the 500 nm level from the AERONET station at Tallahassee, Florida (triangle in A) from the beginning of June to 10th July to show the air quality before and after the dust storm Godzilla. (C) Carbonaceous (CA) river detected during the Amazon forest fire on 08/18/2019 at 1200 UTC from MERRA 2 data. (D) same as in B but over the AERONET station located at São Paulo (triangle in C).

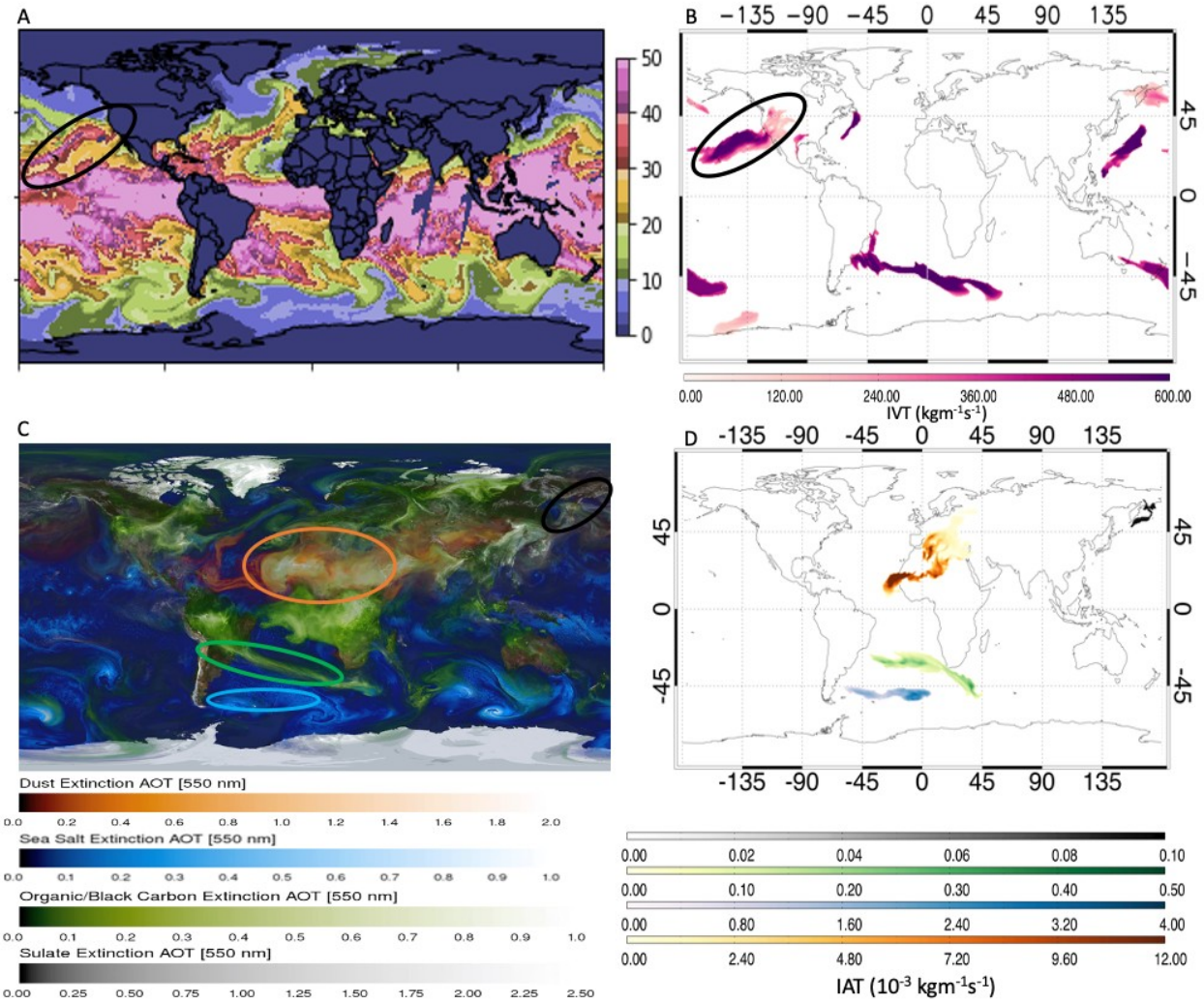

Figure 1(A) SSMI/S satellite observation of integrated water vapor (IWV; mm) for 02/06/2017 showing signatures of ARs. (B) ARs detected based on integrated water vapor (IVT; $kgm^{-1}s^{-1}$) on the same day. The AR corresponding to the region of enhanced IWV marked by the ellipse in (A) was responsible for notable landfall impact over the US West Coast. (C) GEOS-FP aerosol extinction AOT for different aerosol species on 08/18/2006 showing signatures of AARs. (D) AARs of different aerosol species detected by the AAR algorithm based on integrated aerosol transport (IAT; $kgm^{-1}s^{-1}$). The IAT-based AARs correspond to regions with high aerosol concentrations marked by the ellipses in (C). Grey: sulfate; Green: Carbonaceous or organic and black carbon; Blue: sea salt; Orange: dust. Color bars show the magnitude of IVT ($kgm^{-1}s^{-1}$) and IAT (10^{-3} $kgm^{-1}s^{-1}$).

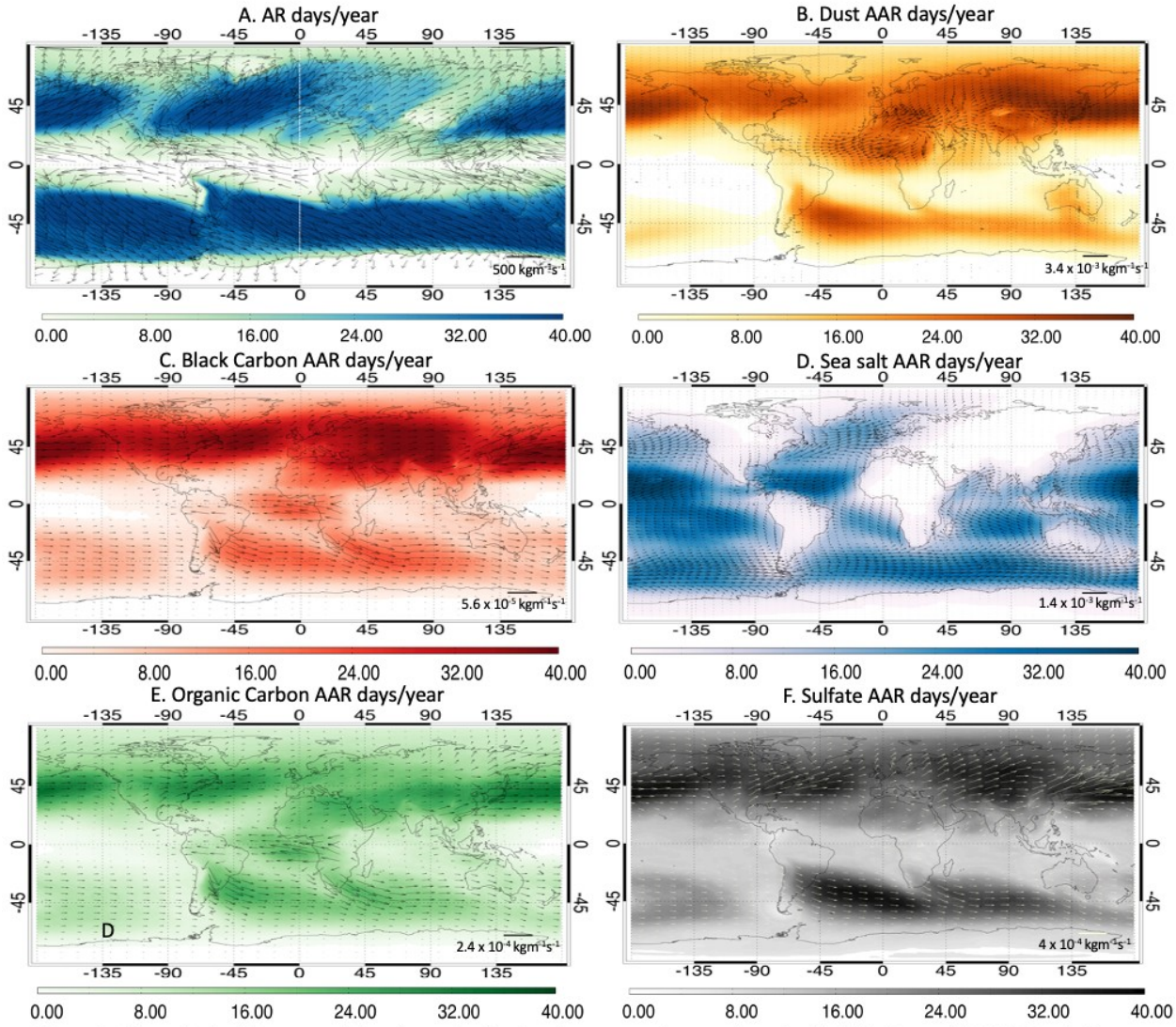

Figure 2. Climatological frequency (days/year; shading) and transport (arrows; kg m^{-1} s^{-1}) of (A) ARs and (B-F) AARs during 1997-2014 based on MERRA-2. (B) Dust; (C) Black carbon; (D) Sea salt; (E) Organic carbon; (F) Sulfate.

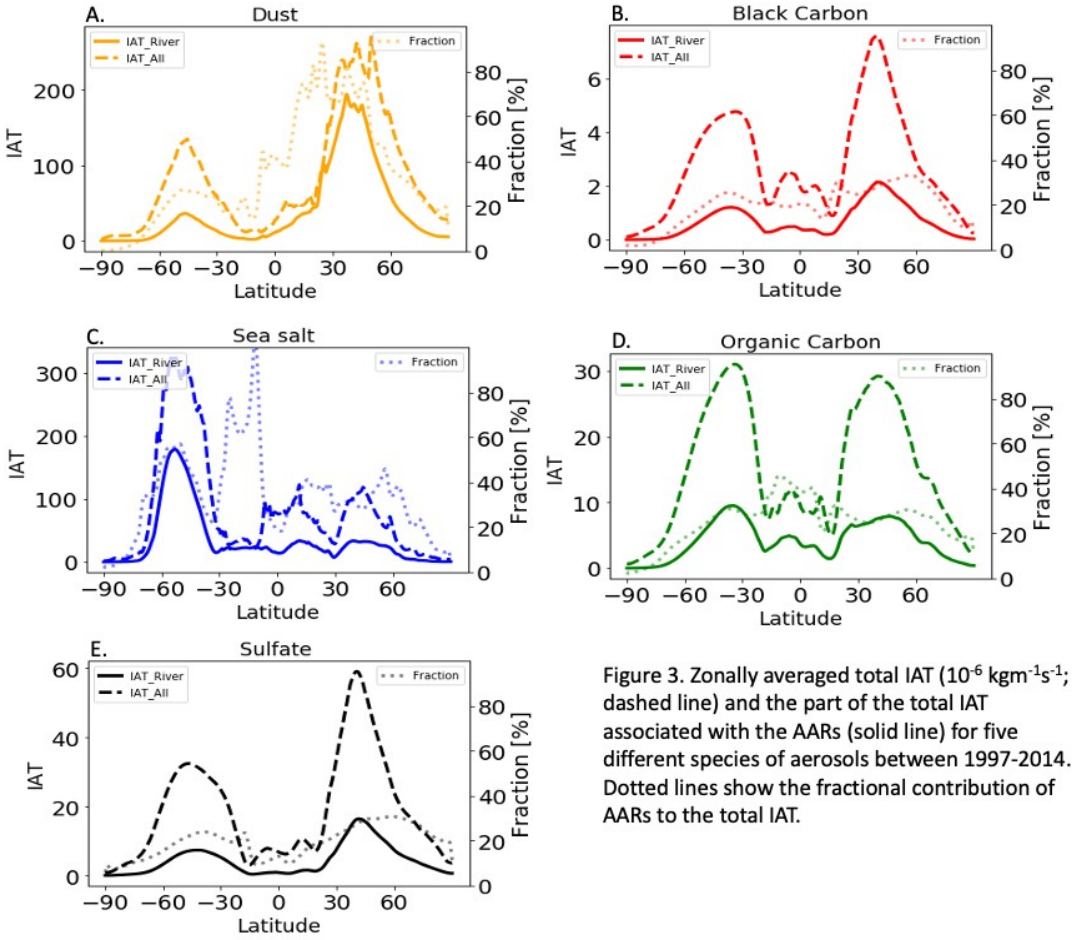

Figure 3. Zonally averaged total IAT (10^{-6} $kgm^{-1}s^{-1}$; dashed line) and the part of the total IAT associated with the AARs (solid line) for five different species of aerosols between 1997-2014. Dotted lines show the fractional contribution of AARs to the total IAT.

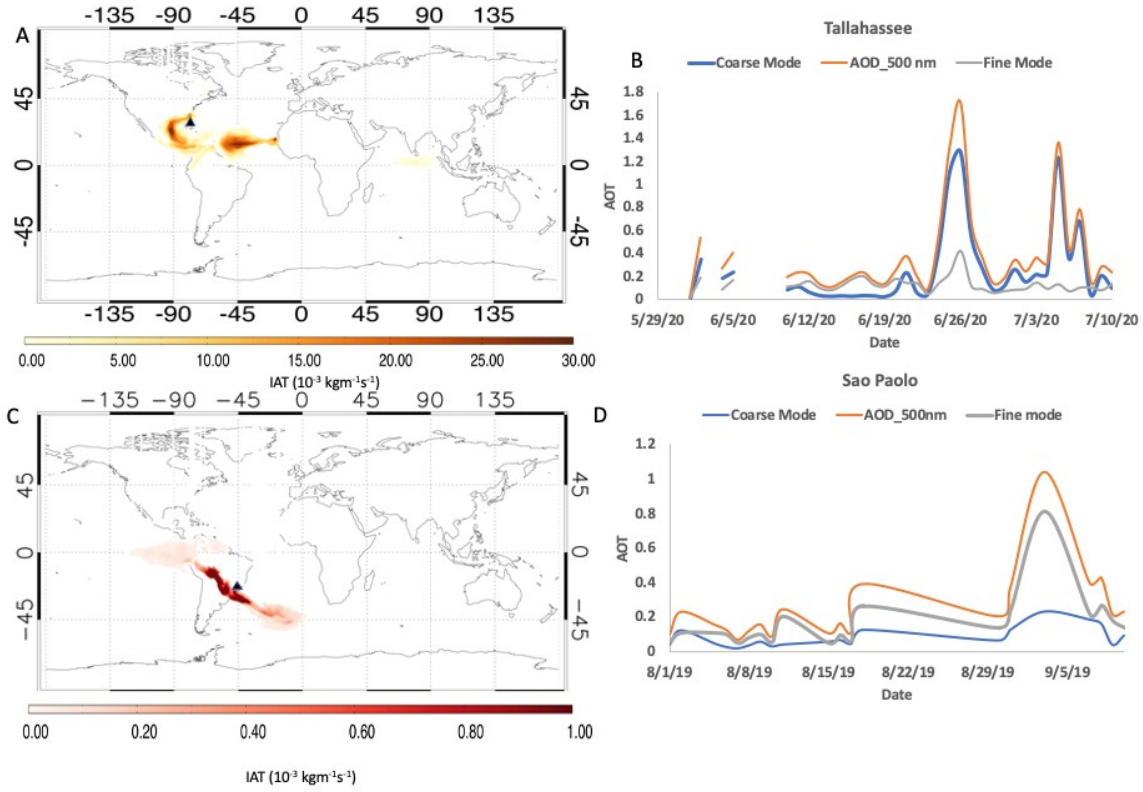

Figure 4. (A) Dust AAR detected by the AAR algorithm from GEOS-FP showing the amount of dusts transported (10^{-3} kg m^{-1} s^{-1}) from the Saharan Desert to Florida on 06/25/2020 at 1330 UTC. (B) Coarse mode AOT, fine mode AOT, and total AOT at the 500 nm level from the AERONET station at Tallahassee, Florida (triangle in A) from the beginning of June to 10th July to show the air quality before and after the dust storm Godzilla. (C) Carbonaceous (CA) river detected during the Amazon forest fire on 08/18/2019 at 1200 UTC from MERRA 2 data. (D) same as in B but over the AERONET station located at São Paulo (triangle in C).

Supplementary Materials:

Figure S1. Feather River discharge at Oroville, CA between 1/1/2017 to 2/28/2017 as reported by the waterdata.usgs.gov.

Figure S2. Sulfate river collocated with the black carbon river detected during the Amazon forest fire on 08/18/2019 at 1200 UTC. The color bar shows the Sulfate IAT in 10^{-3} $kgm^{-1}s^{1}$.

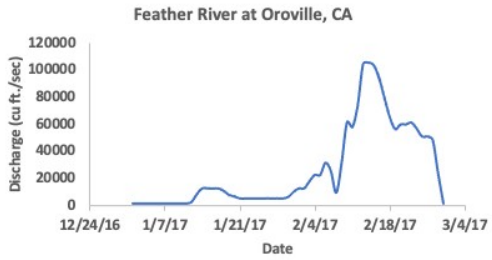

Figure S1. Feather River discharge at Oroville, CA between 1/1/2017 to 2/28/2017 as reported by the waterdata.usgs.gov.

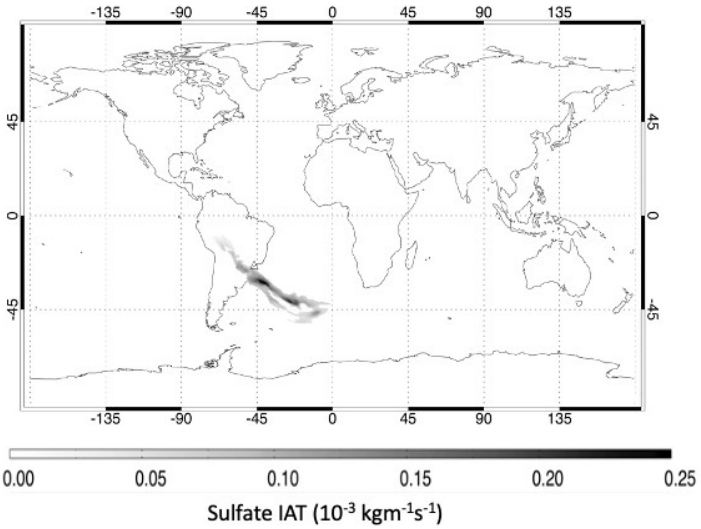

Figure S2. Sulfate river collocated with the black carbon river detected during the Amazon forest fire on 08/18/2019 at 1200 UTC. The color bar shows the Sulfate IAT in 10^{-3} $kgm^{-1}s^{-1}$.